Printed in U.S.A.

76-WA/GT-1

an ASME publication

$3.00 PER COPY
$1.50 TO ASME MEMBERS

Digital Simulation of Fixed and Variable Geometry Free Gas Turbine Engines Based on Quasi-Steady Approach[1]

M. HIRSCH

Instructor

D. ADLER

Senior Lecturer

J. DAYAN

Senior Lecturer

Technion-Israel Institute of Technology,
Department of Mechanical Engineering,
Technion City,
Haifa, Israel

The steady and quasi-steady performance of free gas turbine engines with fixed and variable geometry is calculated. The method is based on the known field of operation of the turbine engine components and, thus, enables to investigate the effect of variations in these components on the overall engine performance. A general mathematical model describing the turbine is developed and solved numerically. A novel iterative algorithm is developed for the solution. It utilizes the nature of the flow through the engine components to improve considerably the speed of convergence of the solution. Results of the calculations are compared with experiments of a small turbine engine, and agreement is good.

[1]This article is a part of M. Hirsch's D.Sc. Thesis supervised by D. Adler and J. Dayan.

Contributed by the Gas Turbine Division of The American Society of Mechanical Engineers for presentation at the Winter Annual Meeting, New York, N. Y., December 5, 1976. Manuscript received at ASME Headquarters July 30, 1976.

Copies will be available until September 1, 1977.

Digital Simulation of Fixed and Variable Geometry Free Gas Turbine Engines Based on Quasi-Steady Approach

M. HIRSCH D. ADLER J. DAYAN

INTRODUCTION

Mathematical models describing the steady and dynamic performance of gas turbine engines are usually based on the a priori known characteristic curves of each of their components (inlet, compressor stages, combustion chamber, coupled turbine stages, free turbine stages, and exhaust pipe).

Each of these elements is described as a macroscopic control volume with uniform inlet and exit distributions of pressure, temperature, etc. In other words, the approach is one-dimensional.

Calculations involving unsteady state conditions for transient simulation purpose, can be divided into two basic approaches. In the first approach, the actual dynamic exit conditions are calculated using a set of differential equations which take into account all the inertia effects in the engine (i.e., mechanical inertia of the rotor and inertia effects of the fluid due to mass, energy, and momentum accumulations [2-3].[1] The second approach is relevant to engines in which the inertia of the rotors is dominant compared to the inertia effects of the through flowing gas. Each of the engine components is represented here by its steady operation conditions through its performance map which is used in a simplified mathematical description of the dynamic performance comprising algebraic equations and tabulated data only. The solution of the mathematical model is based on an iterative procedure along the entire engine. There is a considerable difference in performance predictions between the two approaches at the initial phase of the engine transient, i.e., during acceleration or deceleration, but these predictions converge after a short period [1]. In this paper, the second approach (dominant rotor inertia) is adopted.

Well-tried iterative methods for the solution of engine models are already known [1, 4, 5]. However, one of the contributions of the present work is the development of an improved algorithm which utilizes the nature of the flow in the engine stages. At low subsonic flows, the independent variable of the performance map of each stage incorporated in the engine model is the flow rate parameter. At high subsonic, sonic, or supersonic flows, the independent variable is chosen to be the pressure ratio. This ensures rapid convergence of the numerical procedure in a manner similar to the method presented by Adler, Hirsch, and Dayan [6]. The advantage of this approach as compared to other is that in complicated multispool engines, the number of calculations per engine component is generally independent from the number of the spools.

The present model requires known performance maps of the engine components. These maps can be either experimental or calculated. In the calculation example described here, experimental performance maps were used, except of the variable geometry free turbine stage for which the performance map was calculated according to Reference [6].

THE MATHEMATICAL MODEL

The mathematical model expresses the effects of the engine operation conditions (coupled and free turbine speeds, fuel flow rate, free turbine nozzle angular position, atmospheric conditions and external load) on the aero-thermodynamic quantities with which the laws of mass, momentum, and energy conservation and the laws of thermodynamics and mechanics are expressed, namely: pressures, temperatures, flow rate, accelerations, and power. The model is formulated to satisfy requirements which are imposed by the operation maps of the various components, by the physical engine limitations (such as compressor stall, turbine inlet temperature, and too rich or too lean fuel-air mixture) and by the convergence

[1] Underlined numbers in parentheses designate References at end of paper.

NOMENCLATURE

c_p = specific heat at constant pressure
G = weight flow rate
H_F = heat combustion
J = moment of inertia
M_c = torque at the coupled turbine shaft required by the compressor
M_L = torque at the free turbine shaft
M_{Load} = torque at the power shaft required by the load
M_{Lout} = torque at the power shaft generated by the free turbine
M_T = torque at the coupled turbine shaft generated by the coupled turbine
N_G = real gas generator speed
N_L = real free turbine speed
N_{Lout} = real power shaft speed
n_G = corrected gas generator speed ($n_G = N_G \sqrt{288/T_{1t}}$)
n_L = corrected free turbine speed ($n_L = N_L \sqrt{288/T_{1t}}$)
n_{Lout} = corrected power shaft speed ($n_{Lout} = N_{Lout}\sqrt{288/T_{1t}}$)
P_L = free turbine shaft power
p = pressure
$Q_{cr,f}$ = diving flow rate between region 1 and 2 (Figs. 4 and 5)
$Q_{cr,r}$ = critical flow rate parameter
Q_2 = a flow rate parameter ($Q_2 = G_A \sqrt{T_{2t}}/P_{2t}$)
Q_{3cc} = a flow rate parameter at the exit of the combustion chamber ($Q_{3cc} = G_g \sqrt{T_{3t}}/P_{3t}$)
Q_{3TG} = a flow rate parameter at the entry to the coupled turbine. Physically $Q_{3TG} = Q_{3cc}$; however, due to the iterative technique they can be different until convergence is achieved
Q_{4TG} = a flow rate parameter at the exit of the coupled turbine ($Q_{4TG} = G_g\sqrt{T_{4t}}/P_{4t}$)
Q_{4TL} = a flow rate parameter at the entry to the free turbine. Physically $Q_{4TL} = Q_{4TG}$; however, due to the iterative technique they can be different until convergence is achieved
Q_{5TL} = a flow rate parameter at the exit of the free turbine ($Q_{5TL} = G_g\sqrt{T_{5t}}/P_{5t}$)
T = temperature

Greek Symbols

α = a flow rate parameter at the inlet to the compressor ($\alpha = \frac{G_A\sqrt{T_{1t}/288}}{P_{1t}/1.013}$)
β = coupled turbine speed parameter ($N_G/\sqrt{T_{3t}}$)
ε = convergence criterion
γ = free turbine speed parameter ($N_L/\sqrt{T_{4t}}$)
η_B = combustion efficiency
η_m = mechanical efficiency
η = efficiency

Subscripts

0 = at atmospheric conditions
1 = at the compressor inlet
2 = at the compressor exit and combustion chamber inlet
3 = at the combustion chamber exit and coupled turbine inlet
4 = at the coupled turbine exit and free turbine inlet
5 = at the free turbine exit and exhaust pipe inlet
6 = at the exhaust pipe exit
A = air
c = compressor
cc = combustion chamber
cr = critical
F = fuel
f = fictitious
G = gas generator
g = gas
L = free turbine
Load = external load
Lout = output shaft of the engine
r = real
T = coupled turbine
t = total

Superscript

* = design point

speed of the iterative numerical procedure.

Each of the components (Fig. 1) is incorporated into the model by its a priori known performance map as shown schematically in Figs. 2, 3, 4, and 5. The inlet and exhaust are modeled in the usual manner. The combustion chamber is modeled by the method described by Hawthorne and Olson (7).

The turbines and the compressor are represented in two alternative ways — one for low subsonic flows and one for high subsonic, sonic, or supersonic flows where the flow is almost or actually choked (Fig. 2). This is done to improv the speed of convergence of the iterative calcu-

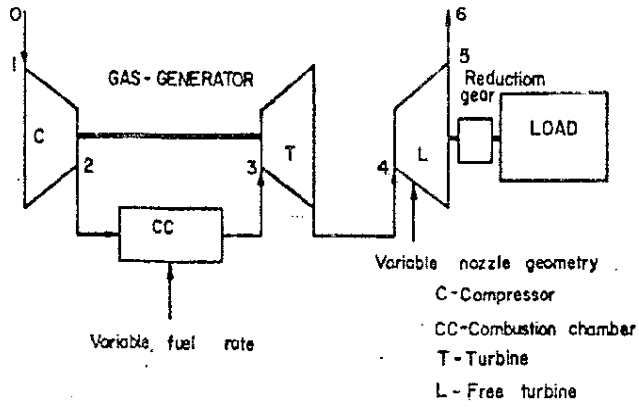

Fig. 1 Schematic diagram of the engine cycle and definition of its components (the numbers define the location indicated by indices 1 to 6)

lation, reducing computation time as is explained later.

Compressor

The contents of the compressor blocks of Fig. 2 are equations (1) to (9) derived from the performance map (Fig. 3). Here the independent variables for the low subsonic flow regime are n_G and α, while at high subsonic, sonic, or supersonic flows, n_G and P_{2t}/P_{1t} are chosen as independent variables as follows:

$$\frac{P_{2t}}{P_{1t}} = \frac{P_{2t}}{P_{1t}}(n_G,\alpha) \qquad \alpha = \alpha(n_G, \frac{P_{2t}}{P_{1t}}) \qquad (1a,b)$$

$$\frac{T_{2t}}{T_{1t}} = \frac{T_{2t}}{T_{1t}}(n_G,\alpha) \qquad \frac{T_{2t}}{T_{1t}} = \frac{T_{2t}}{T_{1t}}(n_G, \frac{P_{2t}}{P_{1t}}) \qquad (2a,b)$$

$$\eta_c = \eta_c(n_G,\alpha) \qquad \eta_c = \eta_c(n_G, \frac{P_{2t}}{P_{1t}}) \qquad (3a,b)$$

Equations (1b), (2b), and (3b) are equivalent to equations (1a), (2a), and (3a), respectively. The choice, which set of equations is selected for the solution depends on the method of convergence of the numerical procedure according to the flow regime as defined by the local Mach number.

$$\frac{P_{2t}}{P_{1t}}_{stall} = \frac{P_{2t}}{P_{1t}}_{stall}(n_G) \qquad (4)$$

or by

$$\alpha_{stall} = \alpha_{stall}(n_G) \qquad (5)$$

Again, equations (4) and (5) are equivalent. Equation (4) is used for high subsonic, sonic,

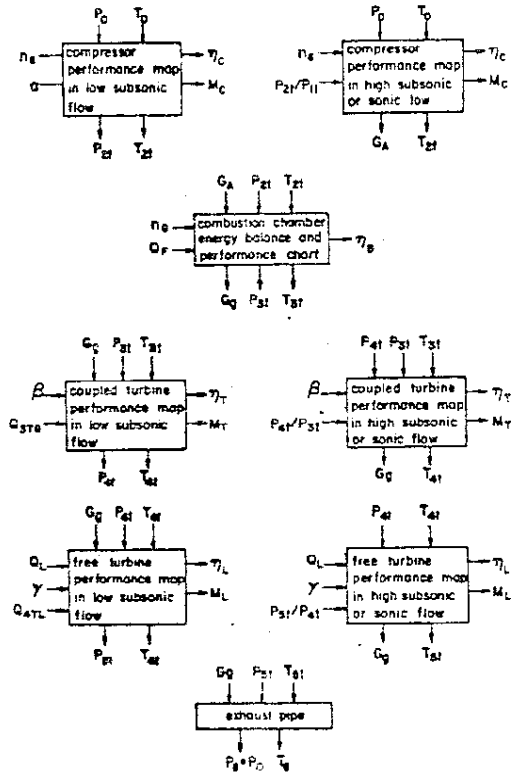

Fig. 2 Diagram of the relationship between the parameters of the engine model (inlet conditions are given at the top of each block, independent variables are given at the left of each block, outlet conditions are given at the bottom of each block, torque and efficiency are given at the right of each block)

or supersonic flows in the compressor and equation (5) for low subsonic flows. Using these equations the exit conditions from the compressor are calculated:

$$P_{2t} = (\frac{P_{2t}}{P_{1t}})P_{1t} \qquad (6)$$

$$T_{2t} = (\frac{T_{2t}}{T_{1t}})T_{1t} \qquad (7)$$

$$G_A = \frac{P_{1t}/1.013}{\sqrt{T_{1t}/288}}\alpha \qquad (8)$$

$$Q_2 = \frac{G_A\sqrt{T_{2t}}}{P_{2t}} \qquad (9)$$

Combustion Chamber

The contents of the combustion chamber block of Fig. 2 are equations (10) to (13). The pressure losses are given by:

$$\frac{P_{3t}}{P_{2t}} = \frac{P_{3t}}{P_{2t}}[(\frac{P_{3t}}{P_{2t}})^*, \frac{G_A}{G_A^*}, \frac{Q_2}{Q_2^*}, \frac{T_{3t}}{T_{3t}^*}] \qquad (10)$$

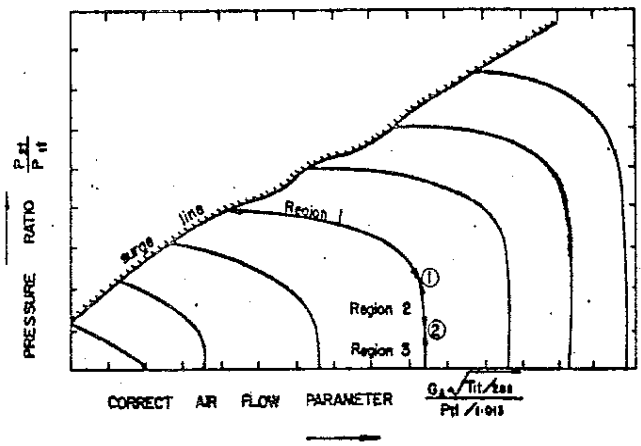

Fig. 3 Typical compressor performance map defining the flow regions (the coordinates of point (1) are $\left[\alpha_{cr,f};\ (P_{2t}/P_{1t})_{cr,f}\right]$ and of point (2) $\left[\alpha_{cr,r};\ (P_{2t}/P_{1t})_{cr,r}\right]$)

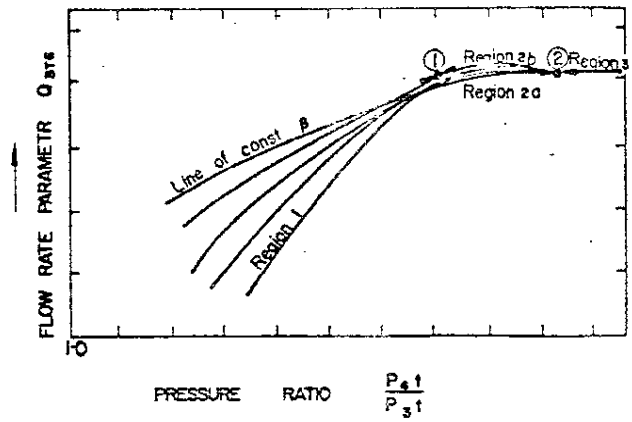

Fig. 4 Typical gas generator turbine performance map defining the flow regions (the coordinates of point (1) are $\left[(P_{4t}/P_{3t})_{cr,f};\ Q_{3cr,f}\right]$ and of point (2) $\left[P_{4t}/P_{3t})_{cr,r};\ Q_{3cr,r}\right]$)

The temperature ratio is calculated from the energy balance

$$G_A \int_{T_{2t}}^{T_{3t}} c_{pA}(T)dT + G_F\left[\int_{T_{1t}}^{T_{2t}} c_{pF_{liquid}}(T)dT + \int_{T_{2t}}^{T_{st}} c_{pF_{gas}}(T)dT\right] = G_F H_F \eta_B \qquad (11)$$

where the combustion efficiency, η_B, is given by

$$\eta_B = \eta_B(G_A, P_{2t}, T_{2t}, N_G, G_F) \qquad (12)$$

Combustion can only exist if

$$\left(\frac{G_F}{G_A}\right)_{\substack{lean\\mixture}}(G_A, P_{2t}, T_{2t}, N_G) < \frac{G_F}{G_A} < \left(\frac{G_F}{G_A}\right)_{\substack{rich\\mixture}}(G_A, P_{2t}, T_{2t}, N_G) \qquad (13)$$

In any other case the flame is unusable.

The relations (12) and (13) are developed according to Hawthorne and Olson [7].

Coupled Turbine

The coupled turbine is described by equations (14) to (18) representing its performance map (Fig. 4). Again the equations are given for the two flow regimes:

Low Subsonic Flows

$$\frac{P_{4t}}{P_{3t}} = \frac{P_{4t}}{P_{3t}}(\beta, Q_{3TG}) \qquad (14a)$$

$$\frac{T_{4t}}{T_{3t}} = \frac{T_{4t}}{T_{3t}}(\beta, Q_{3TG}) \qquad (15a)$$

High Subsonic, Sonic, Supersonic Flows or

$$Q_{3TG} = Q_{3TG}(\beta, \frac{P_{4t}}{P_{3t}}) \qquad (14b)$$

$$\frac{T_{4t}}{T_{3t}} = \frac{T_{4t}}{T_{3t}}(\beta, \frac{P_{4t}}{P_{3t}}) \qquad (15b)$$

Equations (14a) and (15a) are equivalent to equations (14b) and (15b), respectively, and are chosen according to the flow regime.

From these equations the exit conditions are calculated:

$$P_{4t} = \left(\frac{P_{4t}}{P_{3t}}\right)P_{3t} \qquad (16)$$

$$T_{4t} = \left(\frac{T_{4t}}{T_{3t}}\right)T_{3t} \qquad (17)$$

$$Q_{4TG} = Q_{4TG}\frac{P_{3t}}{P_{4t}}\sqrt{T_{4t}/T_{3t}} \qquad (18)$$

Free Turbine

The free turbine is represented by the following equations describing its performance map. A distinction is made between fixed geometry turbines and variable geometry turbines with adjustable nozzle blades.

Fixed Geometry Turbine. The model here is similar to the model describing the coupled turbine:

$$\frac{P_{5t}}{P_{4t}} = \frac{P_{5t}}{P_{4t}}(\gamma, Q_{4TL}) \qquad Q_{4TL} = Q_{4TL}(\gamma, \frac{P_{5t}}{P_{4t}}) \qquad (19a,b)$$

$$\frac{T_{5t}}{T_{4t}} = \frac{T_{5t}}{T_{4t}}(\gamma, Q_{4TL}) \qquad \frac{T_{5t}}{T_{4t}} = \frac{T_{5t}}{T_{4t}}(\gamma, \frac{P_{5t}}{P_{4t}}) \qquad (20a,b)$$

Equations (19a) and (20a) are equivalent to equations (19b) and (20b), respectively. Here again, the choice between equations (19a), (20a), and (19b), (20b), depends on the flow regime.

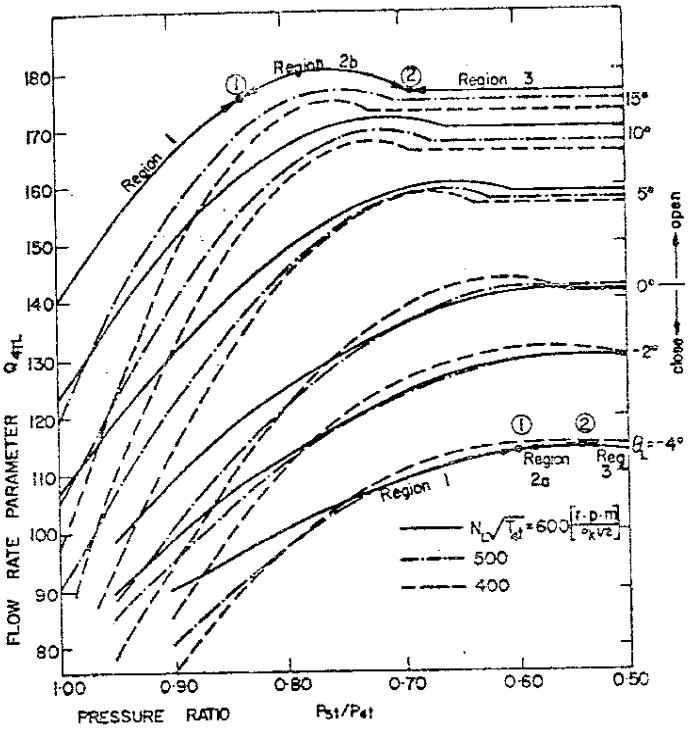

Fig. 5 Calculated variable geometry free turbine performance map defining the flow regions (the coordinates of point (1) are $\left[\left(P_{5t}/P_{4t}\right)_{cr,f}, Q_{4cr,f}\right]$ and of point (2) $\left[\left(P_{5t}/P_{4t}\right)_{cr,c}, Q_{4cr,c}\right]$)

Variable Geometry Turbine.

$$\frac{P_{5t}}{P_{4t}} = \frac{P_{5t}}{P_{4t}}(\theta_L, \gamma, Q_{4TL}) \qquad Q_{4TL} = Q_{4TL}(\theta_L, \gamma, \frac{P_{5t}}{P_{4t}}) \qquad (21a,b)$$

$$\frac{T_{5t}}{T_{4t}} = \frac{T_{5t}}{T_{4t}}(\theta_L, \gamma, Q_{4TL}) \qquad \frac{T_{5t}}{T_{4t}} = \frac{T_{5t}}{T_{4t}}(\theta_L, \gamma, \frac{P_{5t}}{P_{4t}}) \qquad (22a,b)$$

Equations (21a) and (22a) are equivalent to equations (21b) and (22b), respectively, and the choice depends on the flow regime.

From these equations the exit conditions are calculated

$$P_{5t} = \left(\frac{P_{5t}}{P_{4t}}\right)P_{4t} \qquad (23)$$

$$T_{5t} = \left(\frac{T_{5t}}{T_{4t}}\right)T_{4t} \qquad (24)$$

$$Q_{5TL} = Q_{4TL}\frac{P_{4t}}{P_{5t}}\sqrt{T_{5t}/T_{4t}} \qquad (25)$$

Exhaust Pipe

The pressure losses are represented by:

$$\frac{P_{6t}}{P_{5t}} = \frac{P_{6t}}{P_{5t}}\left[\left(\frac{P_{6t}}{P_{5t}}\right)^*, \frac{Q_{5TL}}{Q^*_{5TL}}, \frac{G_g}{G^*_g}\right] \qquad (26)$$

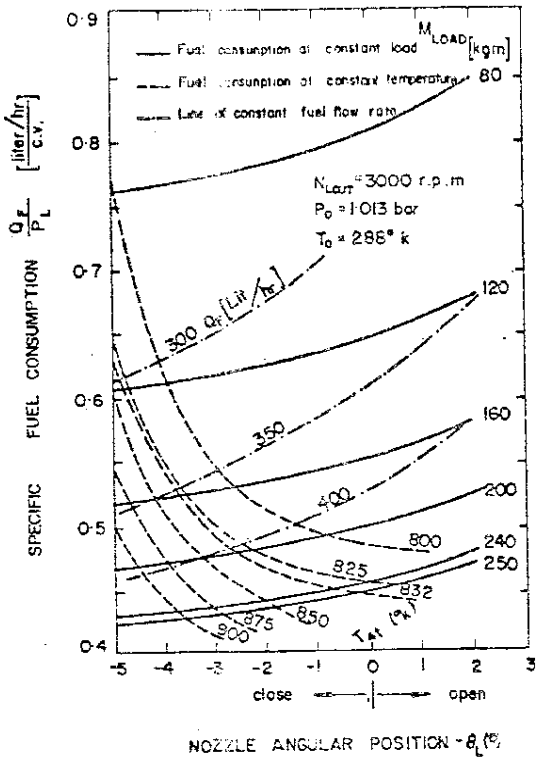

Fig. 6 Flow chart of the computer program

Further, the ratio between the stagnation and static pressures is:

$$\frac{P_6}{P_{6t}} = \frac{P_6}{P_{6t}}(Q_{5TL}, \frac{P_{6t}}{P_{5t}}) \qquad (27)$$

Equations (1) to (27) yield a correct solution if, and only if, the following conditions are satisfied:

$$Q_{3TG} = Q_{3cc} \qquad (28)$$

$$Q_{4TL} = Q_{4TG} \qquad (29)$$

$$P_6 = P_o \qquad (30)$$

As already mentioned, the solution is subjected to a number of physical restrictions imposed on the mathematical model.

(a) Compressor stall is avoided by satisfying

$$\frac{P_{2t}}{P_{1t}} < \frac{P_{2t}}{P_{1t}}_{stall}(n_G) \qquad \text{if} \qquad \left[\frac{\partial(P_{2t}/P_{1t})}{\partial a}\right]_{stall} < 0 \qquad (31)$$

or when the local Mach number is low, by

$$a > a_{stall}(n_G) \qquad (32)$$

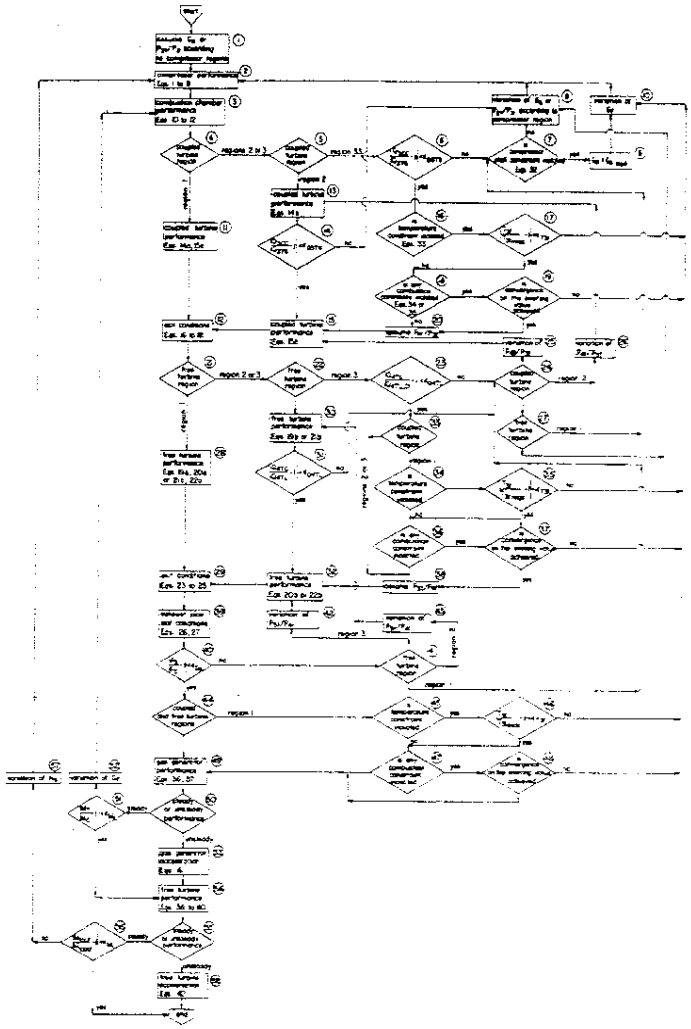

Fig. 7 Calculation paths for the various combinations of the flow regions. (The numbers in the squares correspond to the numbers of the blocks in Fig. 6)

(b) Turbine inlet temperature above the maximum temperature limit is avoided by

$$T_{3t} < T_{3t_{max}} \qquad (33)$$

(c) Combustion flame instability due to rich mixture is avoided by

$$\frac{G_F}{G_A} < \frac{G_F}{G_A}_{\substack{\text{rich}\\ \text{mixture}}} (G_A, P_{2t}, T_{2t}, N_G) \qquad (34)$$

(d) Combustion flame instability due to lean mixture is avoided by

$$\frac{G_F}{G_A} > \frac{G_F}{G_A}_{\substack{\text{lean}\\ \text{mixture}}} (G_A, P_{2t}, T_{2t}, N_G) \qquad (35)$$

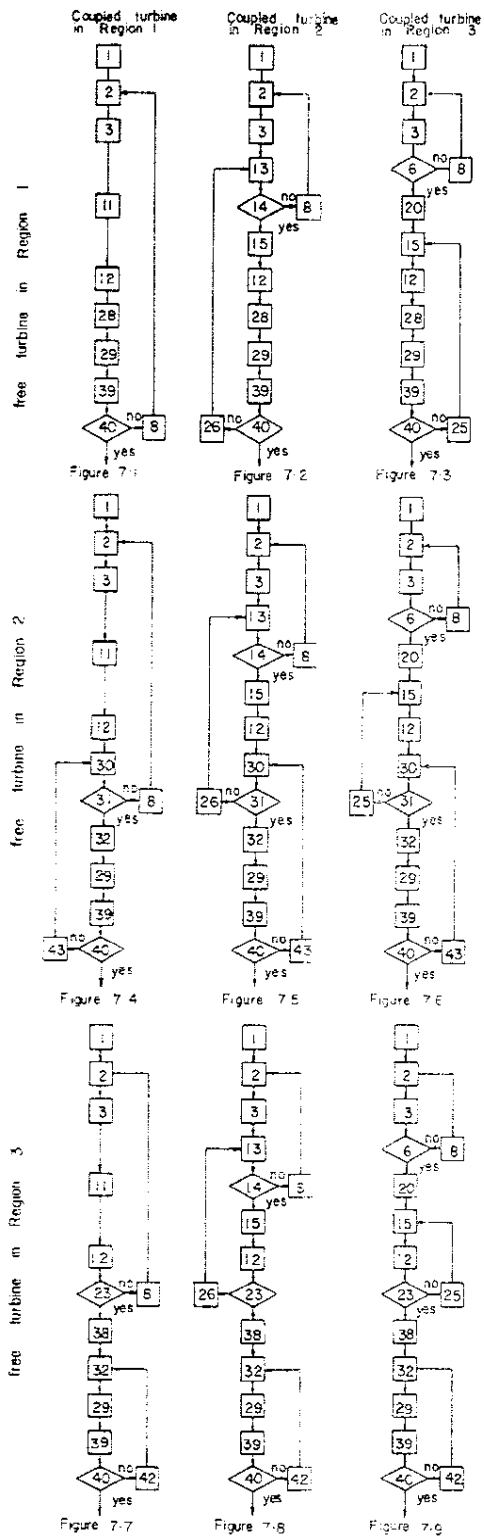

Fig. 8 Specific fuel consumption as a function of θ_L with the load the fuel flow rate and the free turbine inlet temperature as parameters (steady-state operation)

Table 1 Summary of Average Number of Iterations Required for the Solution of the Present Example

Free Turbine Region \ Coupled Turbine Region	1	2	3
1	4-5	5-6	4-5
2	5-6	7-8	5-6
3	4-5	5-6	4-5

If one of these conditions is violated a limiting fuel flow rate is calculated iteratively and then imposed on the solution in such a way that the previously violated condition is satisfied.

If more than one of the three foregoing conditions a, b, or c are violated, the smallest of the calculated fuel flow rates required to satisfy the violated conditions is imposed on the solution.

Knowing all the inner-thermodynamic conditions of the engine, the torques of the gas generator and of the free turbine can be calculated. The following equations are applied:

Compressor

$$M_C = 4077.5 \frac{G_A}{N_G} \int_{T_t}^{T_{2t}} c_{p_A}(T)dT \qquad (36)$$

Coupled Turbine

$$M_T = 4077.5 \frac{G_g}{N_G} \int_{T_{4t}}^{T_{3t}} c_{pg}(T, \frac{G_F}{G_A})\, dT \qquad (37)$$

Free Turbine

$$M_L = 4077.5 \frac{G_g}{N_L} \int_{T_{5t}}^{T_{4t}} c_{pg}(T, \frac{G_F}{G_A})\, dT \qquad (38)$$

The torque at the power shaft

$$M_{Lout} = M_L(\frac{N_L}{N_{Lout}}) \cdot \eta_{mL} \qquad (39)$$

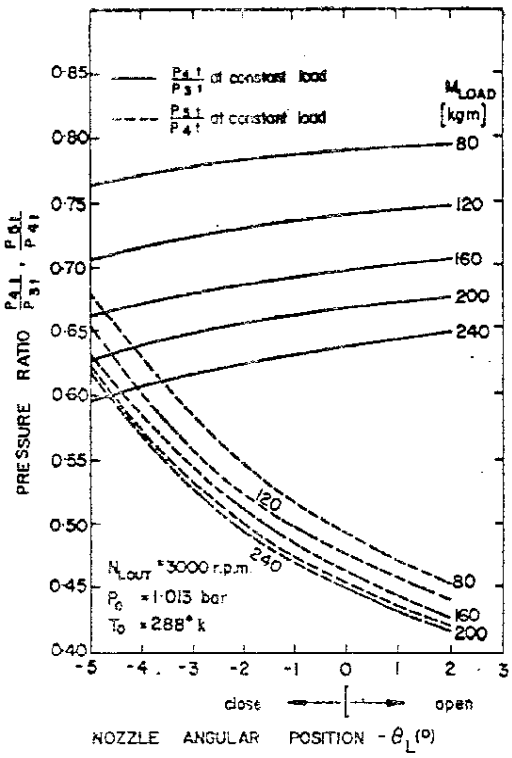

Fig. 9 Pressure ratios as a function of θ_L with the load as parameter (steady-state operation)

The power at the power shaft

$$P_L = \frac{M_L N_L}{716.2} \qquad (40)$$

Thus, the accelerations are as follows:

Gas Generator Acceleration

$$\frac{dN_c}{dt} = \frac{M_T \eta_{mT} - M_c/\eta_{mc}}{(2\pi/60)J_G} \qquad \text{when} \quad \frac{dN_G}{dt} > 0 \qquad (41)$$

Power Turbine Acceleration

$$\frac{dN_{Lout}}{dt} = \frac{M_{Lout} - M_{Load}}{(2\pi/60)J_L} \qquad (42)$$

PROCEDURE OF THE NUMERICAL SOLUTION

The numerical procedure is based on the ideas first applied in a previous paper (6), where rapid convergence of the iterative calculation was ensured by utilizing the nature of the flow regions in the engine components. As shown in Figs. 4 and 5, each curve of the diagrams can be divided into three regions:

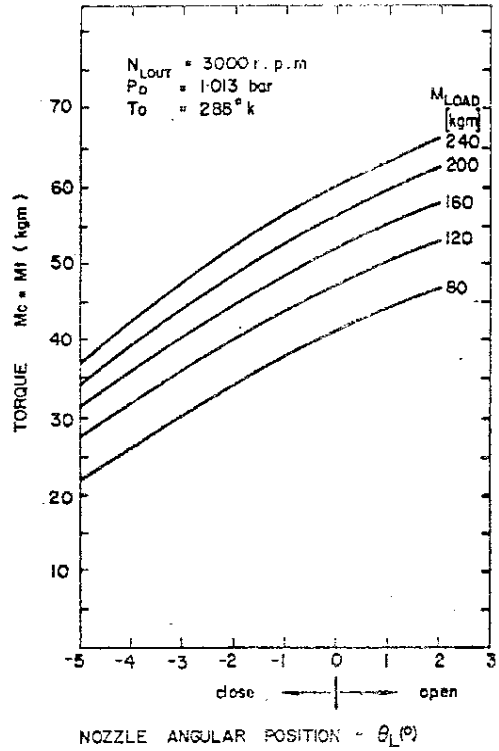

Fig. 10 Gas generator torque as a function of θ_L with the load as parameter (steady-state operation)

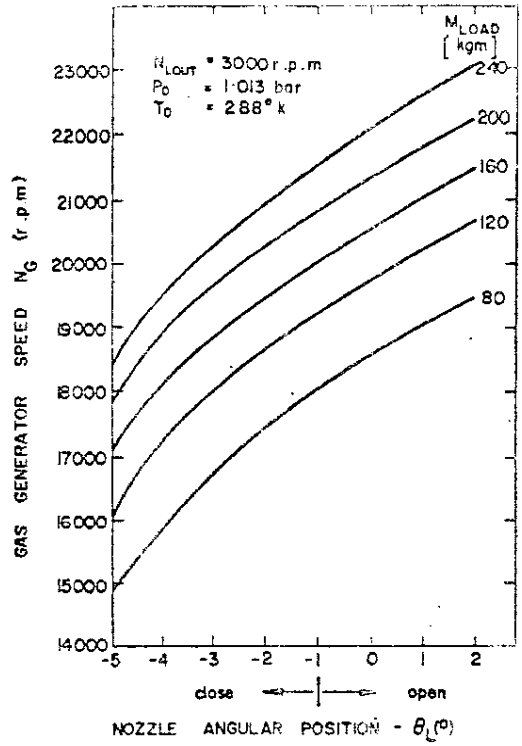

Fig. 11 Gas generator speed as a function of θ_L with the load as parameter (steady-state operation)

Region 1 (Low Subsonic Flows)

In this region, the slope of the curve in Figs. 4 and 5 is steep. Thus, the best choice of the independent variable for rapid convergence is Q_{3TG} or Q_{4TL} as this prevents, automatically, violation of the flow compatibility throughout the entire engine. In other words, this ensures that equations (28) and (29) are always satisfied without necessity for iterations. Consequently, equations (14a), (15a), and (19a), (20a), or (21a), (22a), are used in the calculations.

As the Mach numbers in this region are not high (Ma<0.8), variations in the flow conditions (temperature, pressure, flow rate, etc.) at a point downstream of one of the turbines, affect the performance of all upstream components relative to the turbine in question.

Region 2 (High Subsonic Flows)

In region 2, the curve is either of a moderate slope or flat. It can also be double valued if the flow rate parameter is the independent variable. Hence, if the independent variable is Q_{3TG} or Q_{4TL}, instability may occur in the iterative solution. This difficulty is overcome by introducing the pressure ratio, P_{4t}/P_{5t} [in equations (14b) and (15b)], or P_{5t}/P_{4t} [in equations (19b) and (20b) or equations (21b) and (22b)], as the independent variable in the iterative procedure. This requires additional iterative loops in the calculations to satisfy the flow compatibility [(equations (28) or (29), or both)] which was satisfied automatically in the calculation of region 1. However, the flow rate parameter in this region is a weak function of the pressure ratio; hence, the increase in the amount of calculations due to the additional iterative loops is not very significant.

In region 2, the flow is highly subsonic; thus, downstream variations in the flow conditions have little effect on the upstream flow conditions.

Two types of performance curves are possible in region 2. These are indicated by 2a and 2b in Figs. 4 and 5. Curves of type 2a increase monotonically to their point of the choked flow. Curves of type 2b have a maximum before decreasing to their point of choked flow. Turbines with fixed geometry, or variable geometry turbines with closed nozzle blades, show performance curves of type 2a (6). In this case, when the pressure ratio is decreased, the nozzle is the first element to reach a choked flow condition. This explains the weak dependence of the flow rate parameters on the pressure ratio, mentioned

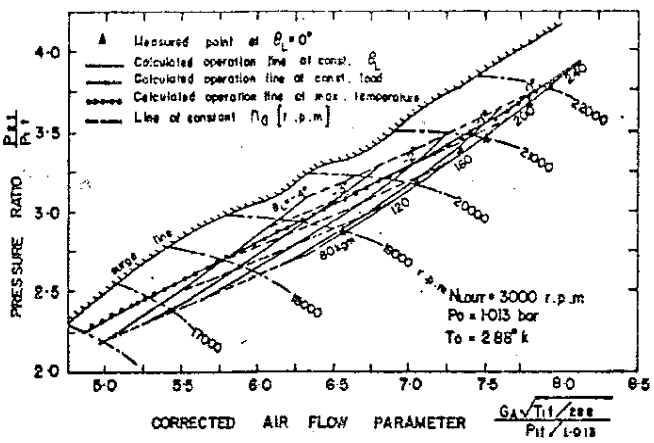

Fig. 12 Calculated operation lines on the compressor map and comparison with measurements at θ_L = 0 deg (steady-state operation)

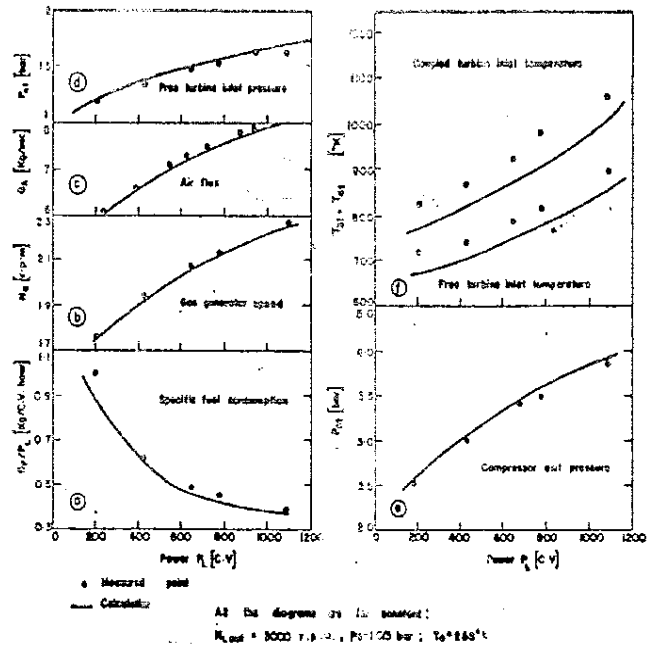

Fig. 13 Comparison between the calculated and the measured performance of the test engine at θ_L = 0 deg (steady-state operation)

in the foregoing. This can be formulated by:

$$\frac{P_{4t}/P_{3t}}{Q_{3TG}}\left|\frac{\partial(Q_{3TG})}{\partial(P_{4t}/P_{3t})}\right| << 1$$

or

$$\frac{P_{5t}/P_{4t}}{Q_{4TL}}\left|\frac{\partial(Q_{4TL})}{\partial(P_{5t}/P_{4t})}\right| << 1$$

Variable geometry turbines with opened nozzle blades may show performance curves with a bump as shown in region 2b of Fig. 5 (6). In this case, the first component to choke when the pressure ratio is decreased is the rotor. Here the flow rate parameter is not as weak a function of the pressure ratio as in the case of turbines having performance curves of type 2a.

This distinction between performance curves of types 2a and 2b is utilized to optimize the convergence method, as is explained later.

Region 3 (Sonic or Supersonic Flows)

In region 3, the flow is completely choked and the performance curves are, therefore, horizontal. The flow rate parameters are equal to their critical values, i.e., $Q_{3TG} = Q_{3cr,r}$, $Q_{4TL} = Q_{4cr,r}$.

In this region the pressure ratio of the coupled and the free turbines must be the independent parameter since $Q_{3cr,r}$ and $Q_{4cr,r}$ are independent of P_{4t}/P_{3t} and P_{5t}/P_{4t}, respectively (Figs. 4 and 5). As the flow here is either sonic or supersonic, upstream flow conditions are completely independent of variations in downstream flow conditions. Thus, the iterative loops are uncoupled as is shown later.

In this case, generally for the coupled turbine:

$$\frac{\beta}{Q_{3cr,r}}\left|\frac{\partial Q_{3cr,r}}{\partial \beta}\right| << 1$$

since the nozzle chokes first when the pressure ratio is reduced (6). A similar condition holds for variable geometry free turbines with closed nozzle blades, i.e.,

$$\frac{\gamma}{Q_{4cr,r}}\left|\frac{\partial Q_{4cr,r}}{\partial \gamma}\right| << 1$$

However, for free turbines, $Q_{4cr,r}$ depends significantly on γ when the nozzle blades are opened (as shown in Fig. 5) since the rotor is the first element to choke when the pressure ratio is reduced.

The three regions defined on the turbine performance maps exist also on the compressor performance map (Fig. 3). The nature of these regions is identical to the corresponding regions on the turbine performance maps (except that the critical flow rate values generally depend on the speed parameter, n). This is utilized to improve convergence in the same manner as in the case of the turbines.

The algorithm which solves the mathematical model is described schematically in Figs. 6 and

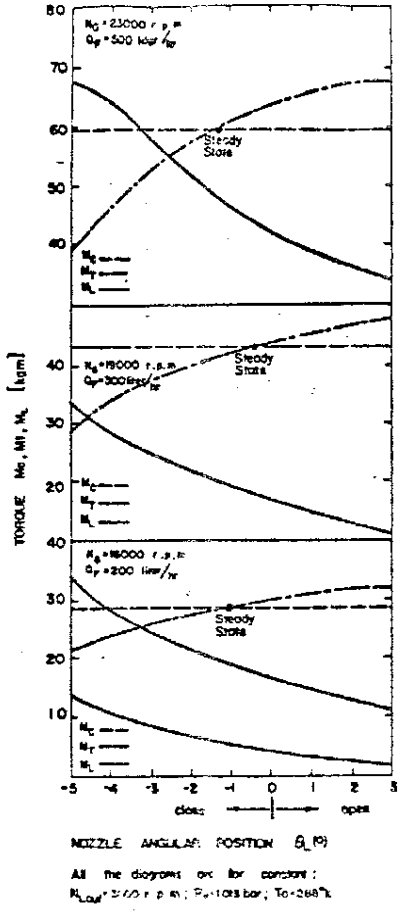

Fig. 14 Torques as function of θ_L at non-steady operation for three sets of constant gas generator speed and fuel flow rate (quasi-steady operation)

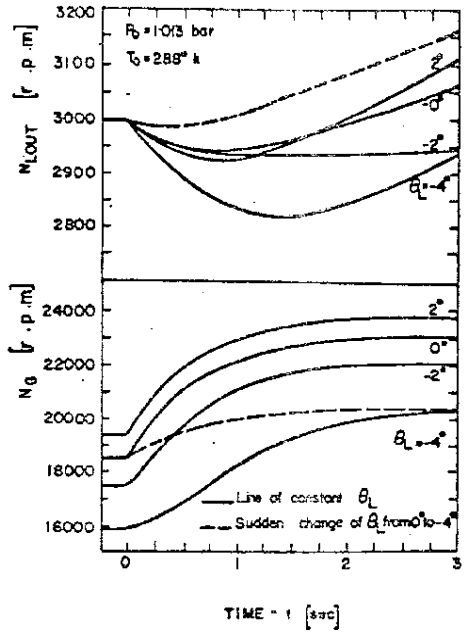

Fig. 15 Transient response of the shaft's speed for a number of θ_L values

7. This algorithm is restricted to engines with single-spool gas generators and single-spool free turbines, which is a particular case of the generalized algorithm ($\underline{8}$) for engines with any number of spools.

Fig. 6 describes the overall flow chart of the algorithm including the iterative loops in which the convergence criterions relevant to the performance map region and the engine constraints are to be satisfied. This algorithm is designed to minimize computation time for a given set of data:

$$P_o \; , \; T_o \; , \; N_o, \; N_{Lout} \; , \; \frac{N_L}{N_{Lout}} \; , \; Q_F \; , \; \theta_L$$

The general solution procedure may include every combination of the flow regions in the engine components pointed out in the foregoing. For each combination, the correct independent parameter on the turbine or the compressor performance map has to be selected to achieve the required rapid convergence. Each combination of performance map regions gives a particular computation path on the flow chart of Fig. 6. The possible paths (not including convergence loops introduced to satisfy the various engine constraints), are described in Figs. 7.1 to 7.9 where the numbers of the blocks as indicated in the flow chart of Fig. 6 are given to describe a particular path. Table 1 summarizes the number of computations per component for a typical engine until convergence is achieved. In each loop, the permissible convergence error is fixed to 0.1 percent. Variations of the iteration variables are carried out with the Newton-Raphson method to reduce computation time.

The number of iterations given in this table is the upper possible bound, because in the calculation of transient operation the initial guess of the iteration variables is a result of a previous calculation. Thus, the initial guess is close to the convergence value reducing the number of iterations required.

The advantages of the present method are clearly pointed out in Figs. 6 and 7, and in Table 1 as follows:

1 In runs in which constraint violations do not occur:

(a) The number of iterations per engine components is independent of the number of

the spools when the turbines operate in the following combinations of regions (where the first number indicates coupled turbine region and the second number indicates the free turbine region): (1;1), (3;1), (1;3), (3;3) (Figs. 7.1, 7.3, 7.7, and 7.9, respectively).

(b) In cases when at least one of the turbines operates in region 2, the number of iterations increases, as can be seen in Table 1, because the loops are coupled (Figs. 7.2, 7.4, 7.5, 7.6, and 7.8). However, the increase in the number of iterations is not very significant since the coupling is weak as was previously described. Moreover, in many cases region 2 coincides with region 3 (as is shown in Figs. 4 and 5 for regions of type 2a). This causes uncoupling of the loops in the program.

2 Frequently, it occurs that while the coupled turbine operates in region 3 one of the engine constraint is violated. In this case, it is not necessary to complete the calculation of the relevant path, until flow compatibility is achieved, and then to satisfy the violated constraint iteratively. The same applies to the case when the coupled turbine operates in region 1 and the free turbine operates in region 3.

(a) If the stall constraint is violated and the coupled turbine operates in region 3 then

$$Q_{3cc} > (1+\varepsilon_{Q_{3TG}})\cdot Q_{3cr,r} = \text{const.}$$

Reduction of G_A in order to decrease Q_{3cc} toward $(1+\varepsilon_{Q_{3TG}})\,Q_{3cr,r}$ leads to $G_A<G_{A_{stall}}$. The solution is then obtained by fixing $G_A = G_{A_{stall}}$ and reduction of G_F until

$$(1-\varepsilon_{Q_{3TG}})Q_{3cr,r} \le Q_{3cc} < (1+\varepsilon_{Q_{3TG}})Q_{3cr,r}$$

(b) When the maximum temperature or the rich air-fuel mixture constraint is violated, G_A and G_F are varied in order to achieve flow compatibility and to satisfy the engine constraint simultaneously. This does not affect the computation of the downstream engine components.

(c) If the lean fuel-air mixture constraint is violated and the coupled turbine operates in region 3, then

$$Q_{3cc} < (1-\varepsilon_{Q_{3TG}})Q_{3cr,r} = \text{const.}$$

Increasing G_A in order to raise Q_{3cc} toward $(1-\varepsilon_{Q_{3TG}})\,Q_{3cr,r}$ increases the violation (makes it worse). The solution in this case is obtained by increasing G_F and reducing G_A until the flow rate compatibility and the lean mixture constraint are simultaneously satisfied. All these calculations do not affect the computation of the downstream engine components as mentioned before.

The foregoing procedures apply to the case when the coupled turbine operates in region 3. They are also correct when the free turbine operates in region 3, while the coupled turbine operates in region 1. In this latter case, flow compatibility is achieved if

$$(1-\varepsilon_{Q_{4TL}})Q_{4cr,f} \le Q_{4TG} < (1+\varepsilon_{Q_{4TL}})Q_{4cr,r}$$

In the course of computing the engine operation, transfer of calculation from the region 1 procedure of an engine component to the procedures for regions 2 or 3 is governed by the value of Q at the entry to the computed component. If $Q>Q_{cr,f}$ for a certain component (each component is characterized by its own $Q_{cr,i}$ — see Figs. 3, 4, and 5) the calculation is transferred from the region 1 procedure to the region 2 procedure. When a component operates in region 2, $|Q/Q_{cr,r}-1|<\varepsilon_Q$ (applicable to region 2a), then the treatment is identical to that used in region 3.

The transfer from region 2 to region 3, from region 3 to region 2, or from region 2 to region 1 is governed by the value of (P_{out}/P_{in}) in the computed component. Critical limiting values for these pressure ratios are known from the performance map of the components, i.e., $(P_{out}/P_{in})_{cr} = f(N/\sqrt{T_{in}})$ for fixed geometry turbines, and $(P_{out}/P_{in})_{cr} = f(\theta_L, N/\sqrt{T_{in}})$ for variable geometry turbines. For example, if at any point in the calculation in region 2, $(P_{out}/P_{in}) > (P_{out}/P_{in})_{cr,f}$, the calculation is transferred to the region 1 procedure.

RESULTS

The present simulation method has been used to simulate the performance of a gas turbine engine manufactured by Beth-Shemesh Engine Ltd.,

Israel (9). The engine (M2TL type) has a rated power of 800 kw at a standard atmospheric conditions (15 C, 1.013 bar). Simulation was made on an IBM 370/165 computer at the Technion, Israel Institute of Technology.

As mentioned the data used in the simulation comprised of test results of the gas generator components and the calculated performance chart of the free turbine calculated according to Reference (6).

Results of the calculations for steady operation at constant free turbine speed of N_{Lout} = 3000 rpm and N_L/N_{Lout} = 5.9 are given in Figs. 8 to 13. Results of the calculations for unsteady points of operation and for transient operation are given in Figs. 14 and 15.

The results are given for a variable geometry free turbine. However, θ_L = 0 deg curves represent the predicted performance of a fixed geometry free turbine.

We shall now discuss the behavior of the main engine performance parameters in the light of the results.

The improvement in specific fuel consumption due to the variable geometry nozzle is shown in Fig. 8. As the nozzle is closed (at constant load), the specific fuel consumption is reduced and the turbine inlet temperature is increased. Therefore, the angular position of the nozzle blades is limited by the temperature constraint of the engine. Hence, operation along this constraint line gives the optimal steady-state performance. Of course, this is only true if other constraints (like compressor stall constraint, etc.) are not violated.

Variation of the angular position of the nozzle affects the pressure drop in the turbines as can be seen in Fig. 9. This, in turn, directly affects the shaft's power distribution.

The output torque of the free turbine increases when nozzle blades are closed and the fuel flow rate is held constant as shown in Fig. 8. It means that the free turbine power increases since the speed of the output shaft is constant in Fig. 8. As was previously mentioned, the increase in the torque (or power) is due to the increase in pressure drop (Fig. 9). It is also due to higher inlet temperatures (Fig. 8) and bigger peripheral velocities of the flow inside the rotor caused by the variation of the velocity triangles (6).

The coupled turbine torque is strongly influenced by its pressure drop. When the turbine is choked, this pressure drop is the dominant effect. It can be seen from Fig. 9 that if the nozzle blades are closed at constant free turbine torque (or power), the pressure drop across the coupled turbine is reduced and, therefore, its torque is reduced (Fig. 10). At steady operation, the compressor torque equals to the turbine torque. Therefore, Fig. 10 can describe the compressor as well.

The speed of the gas generator is given in Fig. 11. It can be seen that when the nozzle blades are closed at constant load, the speed is reduced to cause the torque reduction of the compressor. This reduction in the compressor torque is required in order to balance the coupled turbine torque.

Fig. 12 describes the operation lines on the compressor map. As explained, the compressor operates at reduced pressure ratios and airflow rates when the nozzle blades are closed at constant output power of the free turbine.

Figs. 12 and 13 show a comparison with experiments for θ_L = 0 deg. The agreement of the calculated results with experiments is good. The biggest relative difference being 6 percent in the free turbine inlet temperature. This includes an inaccuracy of 4 percent in the predicted free turbine performance (6).

Torques as functions of the angular position of the nozzle blades at unsteady operation are given in Fig. 14. Here the coupled turbine speed and the fuel flow rate can be varied, while the speed of the free turbine is kept constant. The compressor torque (M_c) remains constant with variation of θ_L. This is because the gas generator operates at the high level of its operation field where the coupled turbine is choked. Hence, any variation of a downstream parameter relative to the coupled turbine does not affect the upstream flow parameters. The coupled turbine torque (M_T) at constant speed decreases when the nozzle blades are closed. This is caused by the reduction of the pressure drop across the turbine which is the only parameter affecting the temperature drop since the turbine is choked and the airflow rate is constant. The torque of the free turbine (M_L) increases with reduction of θ_L because of the same reasons affecting the torque at steady-state operation as mentioned in the foregoing.

Transient response due to sudden gross variation of the load, fuel flow rate, and nozzle blades angular position are given in Fig. 15. Here the load is changed as a step function from 32 to 100 percent of its rated value. Fuel flow rate in each run is the highest possible subject to the engine constraints and maximum fuel constraint.

The response is described for several constant angular positions of the nozzle blades and

also for a case where the nozzle blades are abruptly closed from θ_L = 0 deg to θ_L = -4 deg. For closed nozzle blades (θ_L = -4 deg), the free turbine response is the worst of all curves shown in Fig. 15. This is due to the fact that the operation line for θ_L = -4 deg, at steady operation, is closest to the stall line (see lines of constant θ in Fig. 12), thus restricting the range of possible variations in fuel flow rate. The best response is obtained when the nozzle blades are suddenly closed from θ_L = 0 deg to θ_L = -4 deg. This is due to the increased torque (see Fig. 14) of the free turbine at the beginning of the transient (at t = 0 sec).

CONCLUSIONS

The present article describes a new calculation method which is illustrated by an example of a variable geometry-free turbine. The iterative calculation method is based on well-known mathematical models of gas turbines; its novelty lies in the convergence technique which utilizes the nature of the flow in the engine components to reduce the number of required iterations, thus saving computation time. The solution of the present algorithm is stable and converges safely for all sets of input data tried and for all the initial values of the iteration variables used. In contrast to the presently known calculation methods, the number of iterations per engine component required by this method is almost unaffected by the engine complexity (e.g., number of spools) due to the convergence procedure used. The engine constraints are easily satisfied without increasing the amount of computations especially when either of the turbines operates under choked flow conditions. The efficiency of the present method as compared to other known calculation techniques becomes more evident when the nonlinearities and the number of degrees of freedom in the performance maps of the engine components are increased. The typical performance map of a variable geometry-free turbine, as shown in Fig. 5, is a good example. The present method is effective especially for engines with turbines having performance maps which are strongly influenced by the normalized speeds β and γ. For engines where this is not the case, the method described in Reference (10), paragraph 8.4, should be preferred.

The example given in this article is based on measured performance maps of all the engine components except of the free turbine which is represented by a calculated performance map according to Reference (6). This demonstrates an important application example of the present method, namely the effect of installing a variable geometry nozzle in an engine previously equipped with fuel control only and fixed nozzle blades.

ACKNOWLEDGMENTS

Part of this work was carried out while M. Hirsch was an engineer at Beth Shemesh Engines Ltd., Israel.

The authors wish to thank Beth Shemesh Engines Ltd. for supplying the experimental data incorporated in this paper.

They wish to mention the valuable help, encouragement, and cooperation of J. Sinai, Chief Design Engineer of Beth Shemesh Engines, as well as the help of A. Halfon of the Technion in the computer work.

REFERENCES

1 Fawke, A. J., and Saravanamutto, H. I. H., "Digital Computer Methods of Prediction of Gas-Turbine Dynamic Response," SAE Paper No. 710-550.

2 Fawke, A. J., Saravanamutto, H. I. H., and Holmes, M., "Experimental Verification of A Digital Computer Simulation Method for Predicting Gas Turbine Dynamic Behaviour," Proceedings of the Institute of Mechanical Engineers, 1972.

3 Seldner, K., Mihaloew, J. R., and Blaha, R. J., "Generalized Simulation Technique for Turbojet Engine System Analysis," NASA, TN D-6610, 1972.

4 Dennison, C., "A Nonlinear Digital Simulation Method Applied to Gas Turbine Dynamics," IFAC, Technical Session 25, Moscow, 1969.

5 Muller, G. S., "Gas Turbine Simulation Using One-Dimensional Flow Relationships," Ph.D. Thesis, University of Manchester, 1969.

6 Adler, D., Hirsch, M., and Dayan, J., "The Prediction of the Performance of Variable Geometry Free Gas Turbines," Israel Journal of Technology, Vol. 11, No. 4, 1973, pp. 253-269.

7 Hawthorne, W. R., and Olson, W. T., eds., Design and Performance of Gas Turbine Power Plants, Oxford University Press, 1960.

8 Hirsch, M., Adler, D., and Dayan, J., "Modified Digital Simulation of Multi-Spool Fixed or Variable Geometry Free Gas Turbine Engines Based on Quasi-Steady Approach," to be published.

9 Sinai, J., and Rozewicz, J., "Design, Development, and Applications of Jet Engine Based 800-kw Gas Turbine," ASME Paper No. 74-GT-38.

10 Cohen, H., Rogers, G. F. C., and Saravanamutto, H. I. H., Gas Turbine Theory, Longman, 1972.